ACS OMEGA

http://pubs.acs.org/journal/acsodf

Article

# 2D/3D Metallic Nano-objects Self-Organized in an Organic Molecular Thin Film

Olga V. Molodtsova, Irina M. Aristova, Dmitrii V. Potorochin, Sergey V. Babenkov, Igor I. Khodos, Serguei L. Molodtsov, Anna A. Makarova, Dmitry A. Smirnov, and Victor Yu. Aristov*

Cite This: *ACS Omega* 2020, 5, 10441−10450

Read Online

ACCESS | Metrics & More | Article Recommendations

**ABSTRACT:** We present the fabrication and investigation of the properties of nanocomposite structures consisting of two-dimensional (2D) and three-dimensional (3D) metallic nano-objects self-organized on the surface and inside of organic molecular thin-film copper tetrafluorophthalocyanine ($CuPcF_4$). Metallic atoms, deposited under ultrahigh vacuum (UHV) conditions onto the organic ultrathin film, diffuse along the surface and self-assemble into a system of 2D metallic overlayers. At the same time, the majority of the metal atoms diffuse into the organic matrix and self-organize into 3D nanoparticles (NPs) in a well-defined manner. The evolution of the morphology and electronic properties of such structures as a function of nominal metal content is studied under UHV conditions using transmission electron microscopy (TEM), high-resolution transmission electron microscopy (HR-TEM), and photoelectron spectroscopy (PES) techniques. Using HR-TEM, we have observed the periodicity of atomic planes of individual silver NPs. The steady formation of agglomerates from individual single nanocrystallites with intercrystallite boundaries is observed as well. PES reveals generally weak chemical interactions between silver and the organic matrix and n-doping of $CuPcF_4$ at the initial stages of silver deposition, which is associated with charge transfer from the 2D wetting layer on the basis of core-level spectra shift analysis.

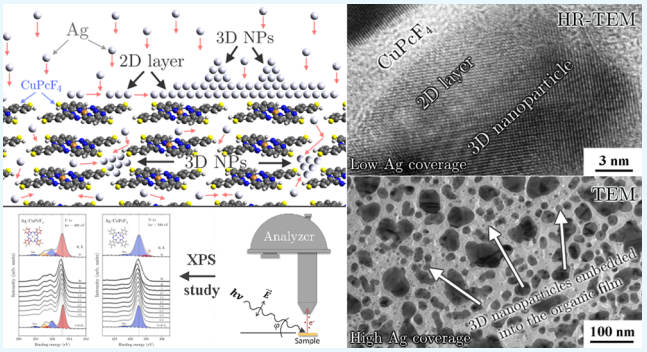


## 1. INTRODUCTION

This study presents the fabrication of nanocomposite structures consisting of two-dimensional (2D) single-crystal silver films grown on the top of an organic matrix copper tetrafluorophthalocyanine ($CuPcF_4$) and three-dimensional (3D) silver nanoparticles embedded in this matrix and investigations of their properties. Such metallic nanoparticles (NPs) can be described as having properties somewhere between those known for atoms and bulk materials. In contrast to the characteristics of atoms and bulk metals, the properties of NPs can strongly depend on their shapes, sizes, etc., especially when reducing the number of metallic atoms in NPs.[1,2] In addition, quantum size effects become more and more pronounced. Therefore, the importance of NPs increases for scientific and technical development.[3,4]

Among metallic NPs, the 2D ones (or so-called 2D metallic layers) occupy a particular place. In our studies on the formation of self-organized nanoparticles in an organic matrix, we have found an interesting phenomenon of the formation of a quasi-2D metallic layer on the surface of an ordered molecular crystal as a result of the metal deposition. Such a quasi-2D metallic layer will be used in the development of new materials[5,6] with new special properties that could be required for numerous applications. Two-dimensional layers of gold, silver, or copper could become indispensable for flexible and transparent electronics (folding displays, electronic paper, clothes, lenses with built-in electronics, etc.).[7−9] However, these materials do not belong to the class of layered ones, and until now, there have been considerable difficulties in producing such ultrathin metal films.[10,11] Considerable success was achieved in solution-based growth of silver 2D nanosheets on air/gel interfaces, which results in large-scale and high-quality 2D silver nanolayer synthesis.[12] Ultrathin metal electrodes could become the technological basis for highly efficient neural interfaces that not only solve a number of medical problems but also bring us closer to the direct integration of the nervous system of living organisms with electronic devices.[13] On the other hand, the current method of growth of self-assembled 2D silver islands on $CuPcF_4$ seems to

Received: January 28, 2020
Accepted: April 16, 2020
Published: April 29, 2020

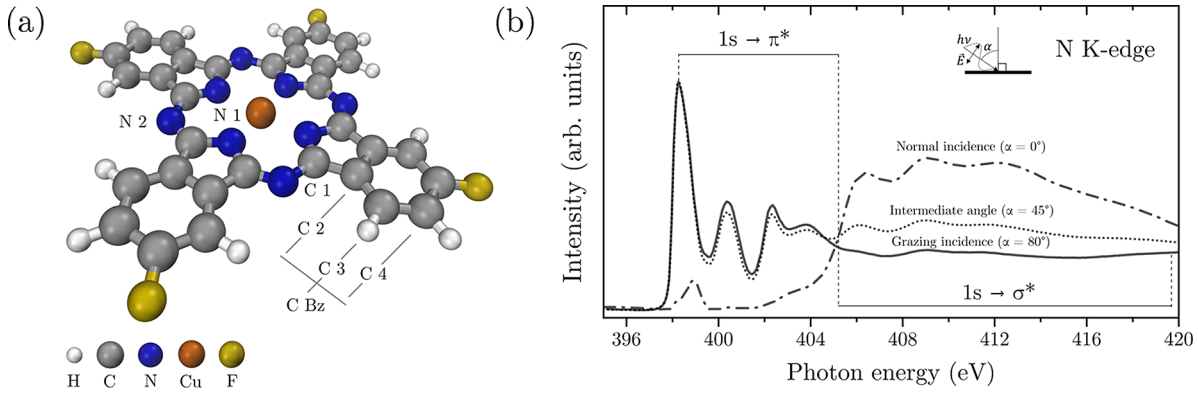


**Figure 1.** (a) Schematic representation of the molecular structure of the $CuPcF_4$ molecule. (b) Angular dependencies of the experimental NEXAFS spectra, confirming that the plane of organic molecules is parallel to the surface of the substrate.

be promising for future application of this phenomenon in the production of mixed-dimensional organic/inorganic heterostructures.[14]

An illustration of the importance of creating nanocomposites—materials consisting of metal nanoparticles with a large variety of physical and chemical properties embedded in an organic matrix—is presented in the article.[15] The properties of such structures will be governed not only by the size and shape of individual NPs but also by their 3D distribution in an ultrathin organic film, reactivity at the interfaces between diverse nanoparticles and organic medium, and by other interface phenomena. Such a combination can radically change the electronic properties of organic wide-band-gap semiconductors, e.g., by applying direct and inverse potentials, the conductivity of such composites can be varied by up to 6 orders of magnitude.[16,17] There is an assumption that such behavior may be caused by the essential charging of nanoparticles. The electric field of charged particles can significantly modify the electronic properties of the molecular thin film.[18−20] Moreover, the charge of NPs, surrounded by a wide-band-gap medium, can keep the change for a long time. As a consequence, there are notable global efforts to produce a new type of memory device for long-lasting storage of data.[21,22] The composites discussed above appear to be increasingly attractive to researchers due to their numerous potential applications.[23,24] In addition to the prospects of high performance, devices using organic-based hybrid schemes can be flexible, which is an additional advantage.[3] Particularly significant is the fact that the development of such hybrid materials is comparatively low in cost and the manufacturing processes are fairly simple. Numerous questions about their properties remain unanswered, and the significance of such studies has grown steadily in the past few years.

To implement complementary logic, semiconductors of both p-type and n-type are needed. Most organic semiconductors, including the majority of thin Pc films, are p-type materials. Therefore, the publications demonstrating that copper phthalocyanine fluorination (formation $C_{32}H_{12}N_8CuF_x$ ($CuPcF_x$), $x$ = 4, 8, 16) causes the lowest unoccupied molecular orbital (LUMO) and the highest occupied molecular orbital (HOMO) to move in the direction of higher binding energies are particularly attractive.[25−27] As a result, the position of the Fermi level in the band gap is shifted toward the LUMO bottom, which is a prerequisite for the change of the hole conductivity in copper phthalocyanine (CuPc) to the electron conductivity in $CuPcF_x$. This means that $CuPcF_x$ is an exclusive material with a wide band gap and delocalized $\pi$ orbitals for organic-based electronic devices.[28] This semiconductor is a highly stable organic compound with a sublimation temperature of about 500 °C, which is relatively high for organic materials. Therefore, it is possible to create controlled molecular fluxes and, thus, to grow thin films in a controlled manner under ultrahigh vacuum (UHV) conditions using the molecular beam epitaxy (MBE) technique. At room temperature, this material has a low vapor pressure, which allows one to study its properties under ultrahigh vacuum conditions.

The structure of a $CuPcF_4$ molecule is schematically shown in Figure 1a. The flat molecule consists of (i) a central copper atom surrounded by four nitrogen atoms (pyrrole, $N_1$), (ii) four other nitrogen atoms (connecting bridges, $N_2$), and (iii) 32 carbon atoms—pyrrole ($C_1$) and benzene ($C_2$, $C_3$, and $C_4$). In addition, if compared to the related copper phthalocyanine, four hydrogen atoms are replaced by fluorine ones.[29] The atomically clean (001) surface of a gold single crystal[30−32] was used as a substrate for growing molecular layers of $CuPcF_4$. The near-edge X-ray absorption fine structure (NEXAFS) technique (see Figure 1b) demonstrates that the grown films are arranged parallel to the surface of the single-crystal Au(001) substrate (see the Experimental Section).

## 2. RESULTS AND DISCUSSION

**2.1. Transmission Electron Microscopy (TEM) Investigations.** The transmission electron microscopy (TEM) investigations prove that after silver deposition onto the organic substrate the processes of self-organization of silver atoms and nanoparticle formation occur, which probably take place due to surface and bulk diffusion. The planar top-view TEM images of hybrid systems developed after silver deposition on the organic semiconductor $CuPcF_4$ for silver coverages of 0.3 (a), 0.7 (b), 1.7 (c), and 3.6 (d) nm are shown in Figure 2a−d. Figure 2e−h presents the histograms of the size distribution of metallic nanoparticles, acquired by the statistical analysis of related top TEM images in Figure 2a−d (550 nanoparticles were analyzed for each histogram).

During the deposition of metal atoms onto an organic substrate, the formation of NPs on the surface or subsurface of the substrate traditionally occurs in two stages: (i) the stage of nucleus formation, in which the nuclei dissociate if they are still below the critical size (otherwise, the nuclei are capable of further growth with nanocluster formation) and (ii) the stage of steady nanoparticle growth, with further ripening and


https://dx.doi.org/10.1021/acsomega.0c00391
ACS Omega 2020, 5, 10441−10450

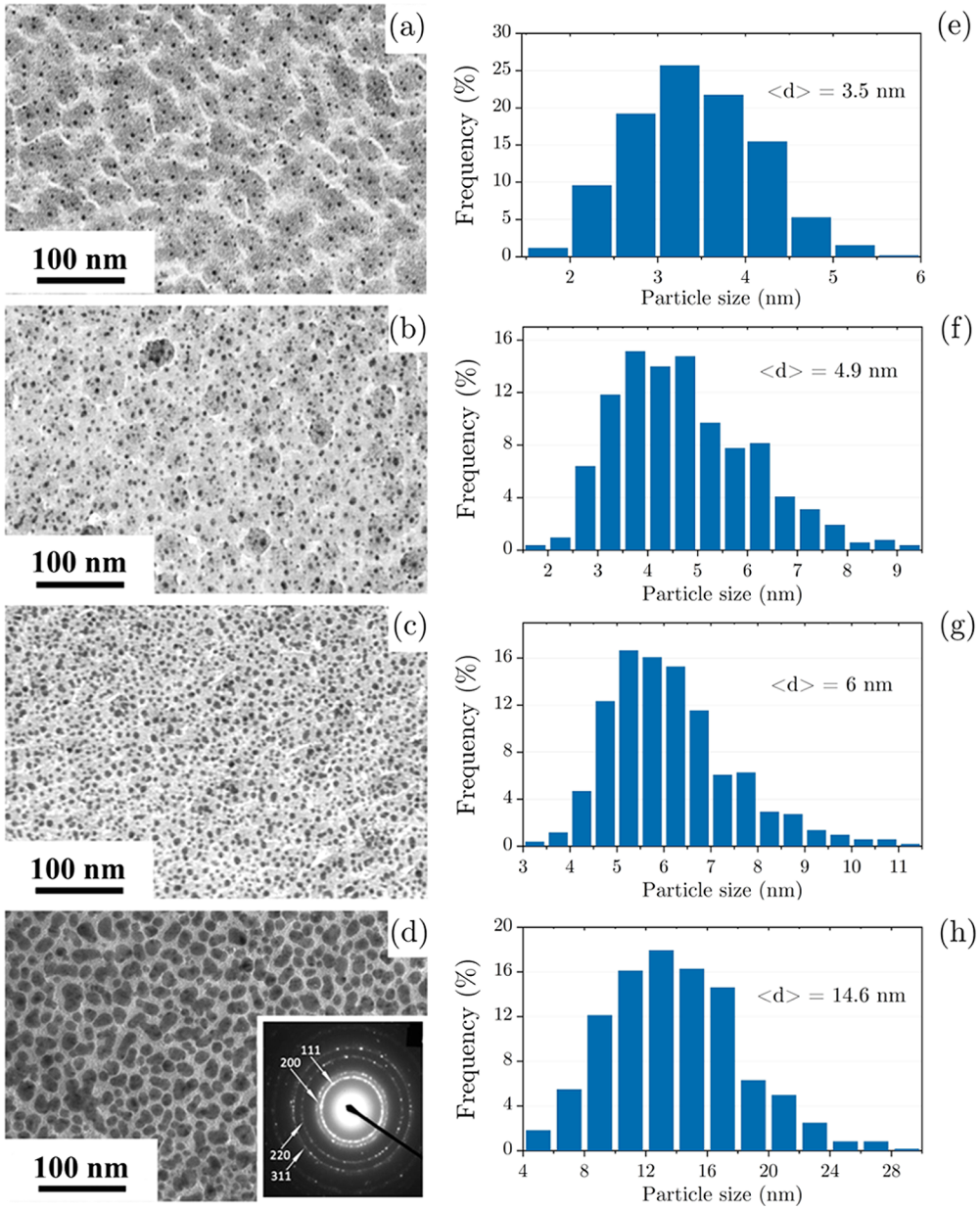


**Figure 2.** (a–d) TEM images (planar top view) of $CuPcF_4$ organic films with distributed silver nanoparticles for a nominal silver deposition of 0.3 (a), 0.7 (b), 1.7 (c), and 3.6 (d) nm. Electron diffraction pattern from an area including several Ag particles for the corresponding deposition can be seen as an inset (d). The inset proves that diffraction originates from silver NPs with a face-centered cubic (fcc) structure. The indices of the first four rings of reflections are given in the image. (e–h) Histograms with size distributions of silver NPs, taken from electron micrographs of (a–d), respectively (550 nanoparticles were analyzed for each histogram). Silver particle distributions are centered on mean values of 3.5 (a), 4.9 (b), 6 (c), and 14.6 nm (d).

coalescence. In the equilibrium theory of heteroepitaxial growth, three growth modes are traditionally distinguished: Frank–van der Merwe (FW), Volmer–Weber (VW), and Stranski–Krastanov (SK). They may be described as layer-by-layer growth (2D), island growth (3D), and layer-by-layer plus 3D island growth, respectively.[33]

Among them, in the SK growth mechanism during the metal atom deposition in the first stage, one observes a process that takes place as a 2D wetting layer formation. As a result, a single monolayer or a coating of several metal layers can be created on the outer surface. In the latter case, it becomes less beneficial thermodynamically. Therefore, the thickness of such a 2D layer (called the SK layer) depends on the amount of deformation inside this layer.[33,34] A condition for the implementation of such a mechanism for the formation of 2D wetting layers is a possible mismatch (less than a few percent) between the lattice constants of the deposited metal and the substrate materials, e.g., organic molecular thin-film $CuPcF_4$.[33,35,36] In the case of silver and CuPc, this mismatch is less than 4% (the tripled lattice constant of silver is 12.24 Å versus 12.7 Å for the organics).[37] We assume that the packing of $CuPcF_4$ molecules on the 5 × 20 superstructure of Au(100) is close to the packing of CuPc due to a similar structure.

Then, after the formation of the SK wetting layer is completed, a second phase takes place: the beginning of the 3D metallic island formation over the 2D wetting layer occurs. The 3D (island) growth mechanism can be implemented in two ways. (i) The first is classical nucleation due to the high


https://dx.doi.org/10.1021/acsomega.0c00391
ACS Omega 2020, 5, 10441−10450

concentration of further adsorbed atoms on the surface of the wetting layer (the growth of islands by this mechanism occurs on a wetting layer of constant thickness). (ii) The second is the nonclassical nucleation of atoms from the wetting layer itself under the action of elastic energy due to the difference in the chemical potentials of the tense atoms in the wetting layer and in the island. In this case, the thickness of the wetting layer should decrease upon nucleation because a part of the atoms of the wetting layer passes into the 3D islands on the top 2D SK layer to, first of all, reduce the elastic energy. The main reason for this phenomenon is that the wetting layer is in an overstressed, metastable state. The origin of islands and their stretching upward is energetically favorable, despite the weakening of the attraction of atoms to the substrate and the increase in the free surface because this leads to a significant decrease in the elastic energy. In other words, this system implements a dislocation-free mechanism for the relaxation of elastic energy caused by a mismatch of the lattices.

Figure 3 presents high-resolution TEM (HR-TEM) images of the structures of the film consisting of silver nanoparticles formed "in or over" an organic semiconductor $CuPcF_4$ for a nominal metal deposition of 0.3 nm. Figure 3a shows the 2D islands of a wetting silver layer. Figure 3b shows another wetting island, which has taken a round shape. Finally, in Figure 3c, we can see the spherical nanoparticle with good crystallinity. Therefore, we observe the results of (i) appearance of the wetting 2D silver layer, (ii) creation of the island with a round shape from that wetting layer, and finally (iii) the 3D spherical nanoparticle formation.

With further deposition of silver atoms, the subsequent growth of nanoparticles is observed. The addition of newly deposited metal atoms to already formed NPs can be accomplished by either direct capture of atoms from the gas phase or by diffusion of adsorbed atoms both inside the matrix and along the surface (under the surface we mean a pure organic substrate and a substrate coated with 2D silver crystals). Figure 4 presents the HR-TEM image, where, as a result of further coating of silver, one sees (A) a layer of the bare molecular matrix, $CuPcF_4$, (B) a 2D ultrathin silver layer grown on the surface of this organic matrix, and (C) a 3D silver crystal, grown on the surface of the 2D silver wetting layer (B), in accordance with the SK model described above.

When the amount of silver deposited on the $CuPcF_4$ organic matrix reaches about 2 nm, the nanoparticles begin to come into contact with each other, and the onset of the process of fusion of metal nanoparticles is observed. This process was studied by modeling in works,[38−40] where it was shown that the initial orientation of the lattice of two nanoparticles affects the entire transient process. Thus, if during the fusion process two nanoparticles have the same lattice orientation, they have an increased contact area and only need a small rearrangement of the lattice and a small relative rotation of the two nanoparticles to combine. With a significant difference in the initial orientation of the lattice of nanoparticles, the initial contact area between the two particles is smaller, the permutation of the atoms should be quite large, and therefore the rotation of one particle relative to the other is stronger. Figure 5a shows an HR-TEM image of the fusion of silver nanoparticles. As a result of coalescence, polycrystalline conglomerates of individual monocrystalline nanoparticles separated by grain boundaries are observed. As a result, regions free of silver nanoparticles are formed in the volume

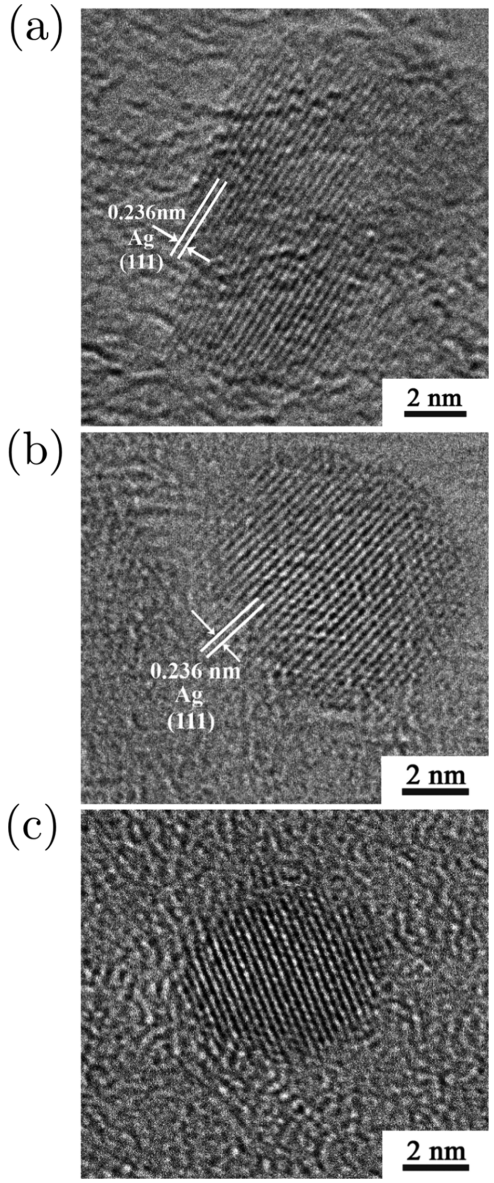


**Figure 3.** High-resolution top TEM image of the $CuPcF_4$ organic film. (a) Island of the wetting layer of silver for a nominal silver deposition of 0.3 nm. (b) Island of silver acquires a round shape. (c) Particle of silver appears to be spherical and has good crystallinity.

and on the surface of the organic film. With further metal deposition, these regions are again filled with diffusing atoms with the subsequent formation of small nanoparticles. As a consequence, the average nanoparticle size can even decrease (see Figure 5b).

**2.2. Photoemission Spectroscopy Study.** Figure 6 shows the experimental spectra of Ag 3*d* (a−c) core levels (CLs) recorded at room temperature, depending on the nominal silver deposition on the surface of the organic semiconductor $CuPcF_4$, up to a thickness of 45 Å. The figure also shows the results of the decomposition of the spectra into components. For small silver depositions from 0.4 up to about 1.5 Å (and a few up to 5 Å), the Ag 3*d* spectrum (Figure 6a−c) has two distinct red and blue components, the intensity ratio of which varies depending on the thickness of the coating from 0.4 up to about 5 Å, and ultimately only one (red) component


https://dx.doi.org/10.1021/acsomega.0c00391
ACS Omega 2020, 5, 10441−10450

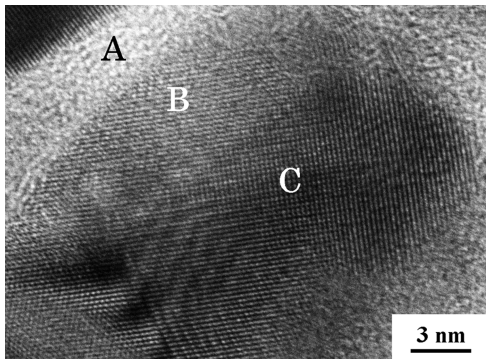


**Figure 4.** High-resolution top TEM image showing: "A"—bare $CuPcF_4$ substrate; "B"—the 2D ultrathin wetting Ag layer, grown at initial Ag deposition according to the SK model; "C"—3D nanoparticle (nanocrystal) on the surface of the 2D silver wetting layer (B).

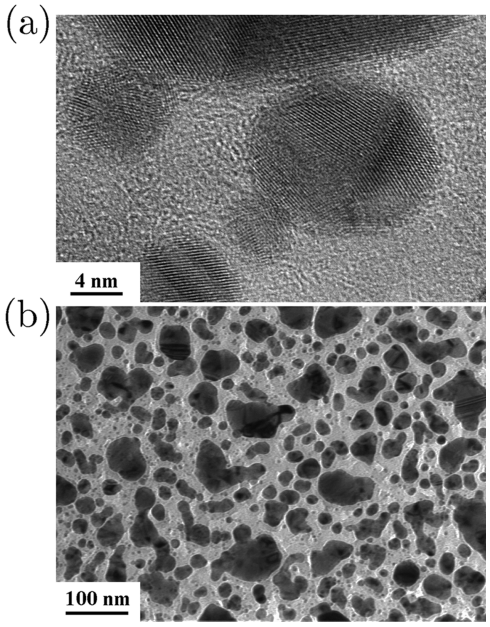


**Figure 5.** (a) HR-TEM top image of the coalescence of silver nanoparticles (JEM 2100, 200 keV). (b) TEM image (planar top view) of a hybrid system consisting of silver NPs in a $CuPcF_4$ organic matrix for a nominal silver deposition of 4.5 nm. The largest dimension of silver nanoparticles formed as a result of the coalescence of metal NPs reaches 100 nanometers.

remains in the region between 5 and 45 Å, which has the characteristic of metallic silver.

The left peak of Ag 3*d* CL (red component) seems to correspond to the already formed nanoparticles, and the right one (blue component) accords to the emission of photoelectrons from 2D silver islands formed on the outer surface of the organic film. As one can see from the spectra with small metal coatings (Figure 6a, spectrum with decomposition for the coating of about 0.4 Å), there are two simultaneous processes: (i) the formation of a wetting 2D layer (less significant blue component) on the outer surface of the organic film (see Figure 3) and (ii) the diffusion of silver atoms into the bulk (more significant red component) of the film to form nanoparticles (see Figure 2a). However, with an increase in the nominal silver coating to 0.9 Å, the formation of the surface wetting layer (a more significant blue component) began to outstrip the direct formation of bulk nanoparticles (a less intense red component) due to the greater surface availability for metal atoms compared to the volume required for diffusion in the film (see Figure 6a, spectrum with decomposition at 0.7−0.9 Å silver).

Further deposition (1.1−1.5 Å in Figure 6b) requires an increase in the total surface of the wetting layer and, as a consequence, nonclassical cases of the nucleation of nanoparticles from the atoms of the wetting layer itself under the action of elastic energy. In this case, the free energy of the island decreases due to the difference in the chemical potentials of the atoms in the wetting layer and in the 3D islands on the top of this SK layer. The evolution of the described process is confirmed by Figures 3−5a. Thus, nanoparticles are formed both by direct diffusion into the volume, with the formation of nanoparticle nuclei and their subsequent growth, and by a transition from a 2D wetting metal layer to 3D nanoparticles formed on the top of the wetting layer with its thickness decreasing (see Figure 4). Further deposition (5−45 Å in Figure 6c) shows the blue component completely disappearing while the red one grows significantly, decreasing in width up to 0.7 eV. The peak position slowly moves from 368.5, which corresponds to ultrasmall NPs, to 368.1 eV, corresponding to metallic Ag 3*d*. The described behavior is clearly seen in Figure 7a. In addition, we should remark that the width of the red peak decreases from 1.2 (0.4 Å) to 0.7 eV (45 Å) finally. The last value is also a reliable characteristic of metallic Ag 3*d*.

Figure 8a−c convincingly provides evidence in favor of the absence of remarkable chemical interaction of silver atoms with atoms of an organic molecule. Indeed with silver atom deposition, we did not observe visible changes of shape in the C 1*s*, N 1*s*, F 1*s*, and Cu 2*p* (Figure 9a) core-level spectra evolution. Figure 8a,c shows the experimental photoemission spectra of the C 1*s* and F 1*s* CLs, recorded at RT, depending on the nominal silver deposition on the surface of the organic semiconductor matrix $CuPcF_4$ up to 45 Å. The decomposition of the spectra reveals only components characteristic of pristine $CuPcF_4$, which basically keeps the width, shape, and position in the process of metal deposition. One can observe only small variations in CL peak positions (it will be discussed below) and a slight increase in full width at half-maximum (FWHM). For example, FWHM of the primary C 1*s* peak increases slightly from 0.62 eV at the initial stages of metal deposition and reaches 0.86 eV at a thickness of about 45 Å, typical for the scattering of electrons of the organic matrix penetrating through the metal overlayer (in our case silver). It is necessary to note one feature associated with the nitrogen N 1*s* CL (see Figure 8b). As is known, in the copper tetrafluorophthalocyanine molecule, there are four nitrogen atoms belonging to the pyrrole rings and connected directly to the central copper atom. Four other nitrogen atoms are bridges connecting pyrrole rings. In a pure film, the binding energies of these atoms coincide and, as a result, the spectrum of N 1*s* cannot be decomposed into the corresponding components. Consecutive deposition of silver on the $CuPcF_4$ thin film with an increase of the nominal thickness up to 45 Å does not lead to a resolution of the peaks, which again displays the weak interaction of silver with the organics. In the case of deposition of more chemically active metals, for example, aluminum, a splitting of the N 1*s* CL peak into two components is observed with a separation of 0.46 eV.[41] The nature of "*R*" in Figure 8b (top spectrum) peak is currently not completely clear.


https://dx.doi.org/10.1021/acsomega.0c00391
*ACS Omega* 2020, 5, 10441−10450

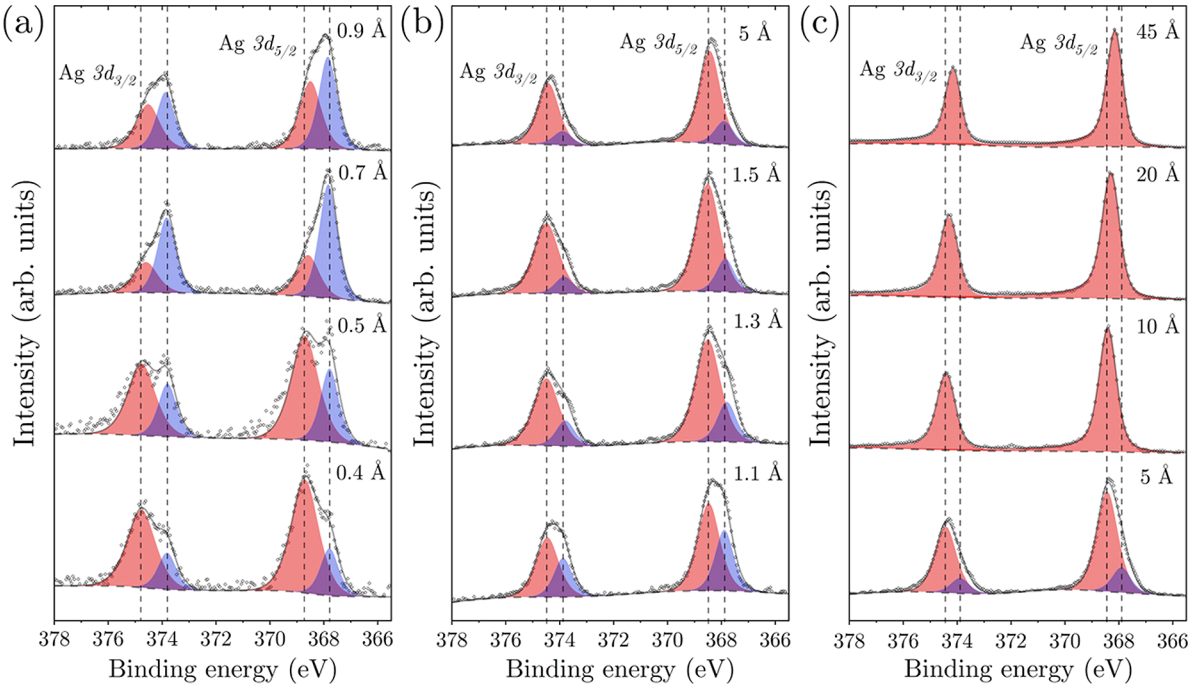


**Figure 6.** Experimental photoemission spectra of the core level of Ag 3*d* (a–c) recorded at room temperature depending on the nominal silver coating on the surface of the organic semiconductor $CuPcF_4$. The nominal silver quantity is shown on the right side of each spectrum in the range of thicknesses from 0.4 to 45 Å. The figure also shows the results of the decomposition of the spectra into two components. The left one (red component) probably originates from already grown 3D nanoparticles, and the right one (blue component) corresponds to the emission of photoelectrons from 2D silver islands formed on the outer surface of the organic film. Detailed analysis of the evolution of both components is found in the text.

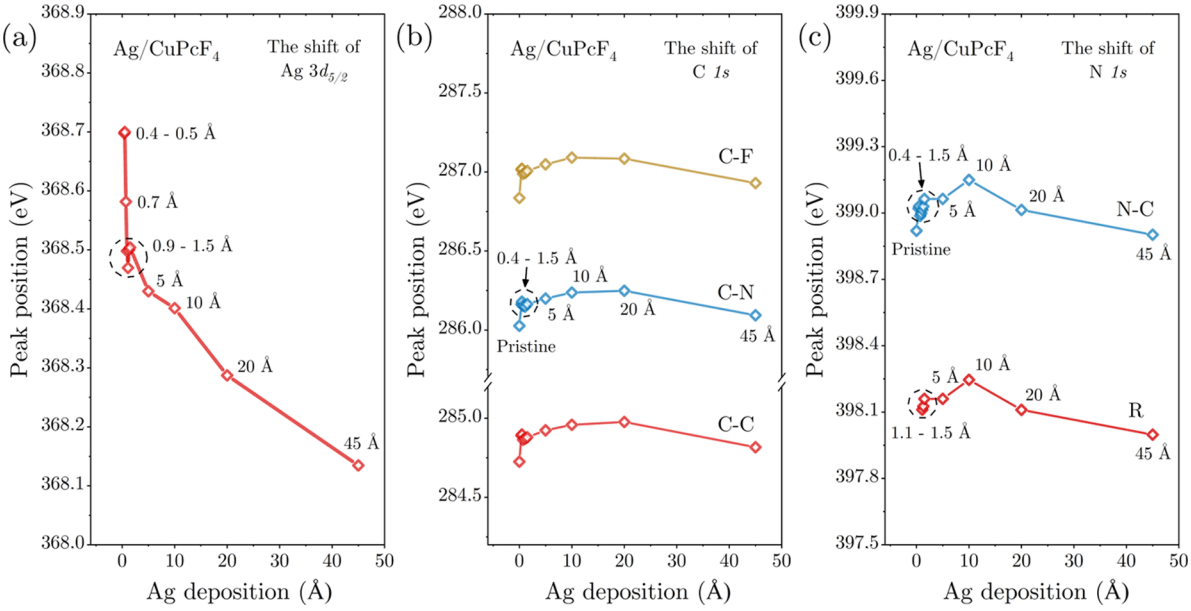


**Figure 7.** Evolution of the peak positions of photoemission spectra of the core levels of Ag 3*d* (a), C 1*s* (b), and N 1*s* (c) recorded at room temperature, depending on the nominal silver coating of the surface of the organic semiconductor $CuPcF_4$. The nominal silver quantity is shown in the vicinity of each experimental point of the peak position in the range of thicknesses from 0 (pure organic film) to 45 Å.

It is worth noting that all CL peaks related to the organic molecules, except Cu 2*p*, exhibit a slight shift toward higher binding energies (n-doping) at the initial stages of deposition, reaching approximately 0.2 eV (Figures 7b,c and 8a–c) at the extreme point (around 10 Å nominal thickness). However, most of the shift is already achieved at 1.5 Å nominal coverage. With further deposition, peak positions move in the opposite direction, toward the Fermi level, and nearly reach the initial state. This means that the positive shift occurs with the existence of the blue peak in Ag 3*d* CL (Figure 6), which we attribute to the 2D wetting layer. We assume this might be considered as an indicator of charge transfer between the following structure and $CuPcF_4$. This statement is supported


https://dx.doi.org/10.1021/acsomega.0c00391
*ACS Omega* 2020, 5, 10441–10450

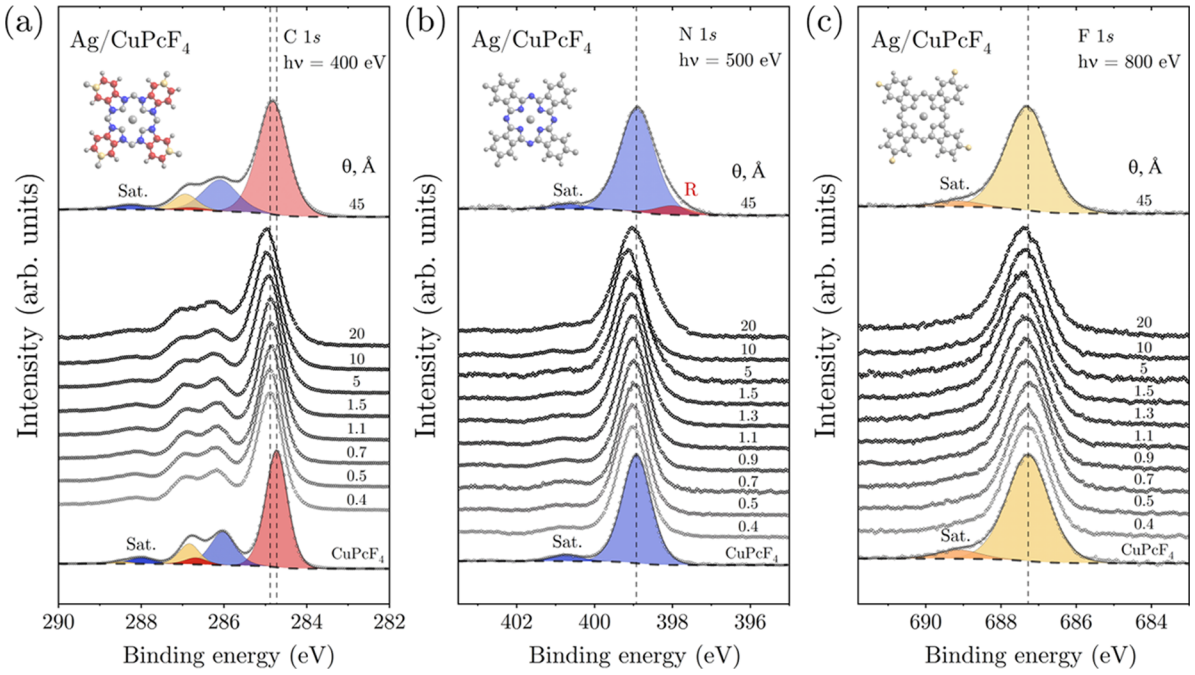


**Figure 8.** Experimental photoemission spectra of the core levels of C 1*s* (a), N 1*s* (b), and F 1*s* (c) recorded at room temperature depending on the nominal silver coating of the surface of the organic semiconductor $CuPcF_4$. The nominal silver quantity is shown on the right side of each spectrum in the range of thicknesses from 0 (pure organic film) to 45 Å. The figure also shows the results of the decomposition of the spectra into components. The inset shows a schematic representation of the $CuPcF_4$ molecule in which the atoms that contribute to the corresponding components of the spectra have the same color.

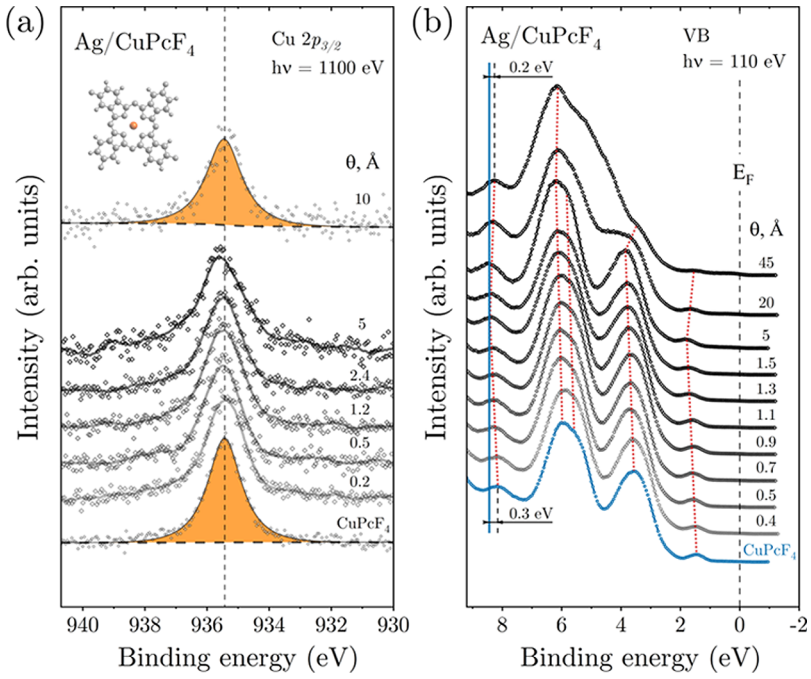


**Figure 9.** (a) Core-level spectra of Cu 2*p* recorded at RT, as a function of metal deposition on the top of the organic film. A schematic representation of the $CuPcF_4$ molecule is shown in the inset. The central atom of the molecule, the copper atom, and the component of the spectra to which it contributes are shown in one color. (b) Valence-band (VB) spectra as a function of metal deposition. To easily track the potential changes in the spectra, they are normalized and are stacked in a vertical direction. The nominal silver quantity is shown on the right side of the panel.

by the fact that the blue peak exhibits an opposite negative shift relative to the component attributed to 3D nanoparticles.

Similar behavior was observed by Lozzi et al.[42] in the case of gold deposition on a CuPc thin film. Valence-band spectra evolution has demonstrated the HOMO shift toward higher binding energies (n-doping) and further recovery back at a nominal thickness of metal deposition comparable to that of our study. However, the same group did not observe any effect on CLs,[43] which is explained by much higher probing depth due to higher photon energy used for the photoemission study.



https://dx.doi.org/10.1021/acsomega.0c00391
ACS Omega 2020, 5, 10441−10450

This fact confirms that the charge transfer occurs at the surface of the thin organic film, and the 2D wetting layer is a prospective candidate for this process.

Figure 9a shows the experimental photoemission spectra of the Cu $2p_{3/2}$ CL recorded at room temperature, depending on the nominal silver coating of the surface of the organic semiconductor $CuPcF_4$ up to 10 Å. The decomposition of the spectra reveals only one component within the whole process of metal deposition, which retains the shape and exhibits a slight shift toward higher binding energies and a small increase in FWHM. The shift of the spectra is less pronounced in comparison to other CL peaks of $CuPcF_4$. This can be justified by higher kinetic energies of photoelectrons (therefore higher probing depth) and lower signal-to-noise ratio (less reliable fitting) because there is only one copper atom out of 57 ones in the organic molecule. The main inference that one can make on the basis of Cu 2*p* CL analysis is that silver atoms do not interact with copper from the middle of the $CuPcF_4$ molecule, which is in contrast to the behavior of non-noble metals.[41,44]

Figure 9b shows the dependence of the evolution of $CuPcF_4$ valence-band spectra on the amount of nominal silver deposition, taken at a photon energy of 110 eV. The red dashed lines indicate the evolution of the valence-band (VB) states, while $E_F$ is marked by a gray one. The analysis was based on the experimental spectra of pristine CuPc[43] and $CuPcF_4$ with[29] and without[45] deposition of gold on top, as well as on the calculations of CuPc VB from the first principles, which could be found elsewhere.[46] With silver deposition up to about 5 Å onto the $CuPcF_4$ thin film, the whole VB spectrum slowly shifts toward higher BE (to about 0.3 eV) involving all of the VB peaks without any noticeable additional structures emerging between HOMO and $E_F$. The overall line shape of the valence features does not show significant changes up to silver coverage of about 5 Å. Increasing silver deposition (Figure 9b, 20 and 45 Å) leads to a reverse shift (about 0.2 eV) of spectra to lower BE, toward the sample Fermi level that correlates in general with the behavior of CLs with a similar deposition amount. The HOMO peak becomes less pronounced with further metal deposition. We have to note that at Ag coverage of above 5 Å (see 20 and 45 Å thicknesses), one should expect (i) silver sp band formation in the region between the Fermi edge and 4 eV BE, while (ii) silver 4d band formation takes place in the region 4−7 eV BE.[47] However, with the highest nominal silver coverage used in our experiment, it is still possible to detect some contribution from organic $CuPcF_4$ thin film in the total VB spectra.

In the case of gold deposition on $CuPcF_4$, one observed a different effect on the position of the VB components.[29] At the minimum nominal deposition thickness of 1 Å, a slight shift toward higher binding energies occurs, while at all further stages of deposition, the spectrum exclusively moves toward the Fermi level, reaching a considerable shift of 0.6 eV, which eventually means p-doping of the thin film. We assume that this effect is due to the fact that gold atoms tend to diffuse deep inside the organic film[32] and not to form a 2D wetting layer, which provides n-doping. Apparently, in the case of silver deposition, a competition between two effects occurs: (1) n-doping by 2D layer and (2) p-doping by 3D nanoparticles.

## 3. CONCLUSIONS

In the current report, we presented the growth of 2D and 3D nano-objects on the surface and inside of an organic $CuPcF_4$ thin film. Based on TEM studies, the origin of 2D Ag islands on the surface of the organic matrix was associated with the 2D wetting layer formation according to the SK mechanism. At the same time, due to the diffusion of silver atoms into the depth of the organic film, 3D nanoparticles are formed in its volume due to self-assembly. TEM and HR-TEM images showed that the evolution of morphology and crystallographic structure of the hybrid system depends on the nominal metal coverage. Ag 3*d* CL spectra analysis has shown the presence of two peaks, which are attributed to the two different types of nano-objects. The one, associated with the 2D layers, shows itself only at the initial deposition stages. Its existence is accompanied by a shift of CL and VB peaks of $CuPcF_4$ toward lower binding energies, which indicates the n-doping of the organic film as a result of charge transfer from the wetting layer. Vanishing of the corresponding peak in the Ag 3*d* spectra almost leads to the recovery of the CL and VB positions. Comparison to gold deposition on the same organic substrate allows assuming that this back movement is justified by the competition of n-doping by 2D layers and p-doping by 3D nanoparticles. The decomposition of the CL spectra reveals only components characteristic of pristine $CuPcF_4$, which basically keep the width, shape, and position in the process of metal deposition. One can observe only small variations in CL peak positions and a slight increase in FWHM, which indicates weak chemical interactions of silver with the organic matrix.

## 4. EXPERIMENTAL SECTION

**4.1. Preparation of the $CuPcF_4$ Thin Film.** A Au(001) crystal was employed as a substrate for the growth of the $CuPcF_4$ thin film. Its purity was achieved by repeated cycles of 1 kV Ar ion bombardment and subsequent annealing at 600 °C under UHV until the well-known superstructure 5×20 appeared on the surface of the gold crystal. This structure was observed by low energy electron diffraction (LEED) and can be formed only on a very clean Au(001) surface.[30−32] The substrate cleanliness was additionally controlled by core-level and valence-band photoelectron spectroscopy using a synchrotron radiation facility, where no traces of carbon, oxygen, or other elements were found.

Highly ordered coatings of up to 22 nm of organic molecular layers of $CuPcF_4$ were grown under UHV (base pressure: $P = (4-8) \times 10^{-11}$ Torr) by the MBE method using specially developed and homemade sources. The orientation and ordering of the grown films were controlled using the NEXAFS technique (see Figure 1b). Figure 1b demonstrates that in the NEXAFS spectra there is a strong dependence of the N 1*s*-$\pi^*$ and N 1*s*-$\sigma^*$ intensities on the incidence angle of a horizontally polarized photon beam. In the case of grazing incidence, when the polarization vector **E** is almost perpendicular to the surface of the substrate, the intensity of N 1*s*-$\pi^*$ transitions shows a maximum, while that of N 1*s*-$\sigma^*$ transitions shows a minimum. If **E** is parallel to the substrate, the intensity ratio is reversed. All this indicates that organic molecules in the grown films are arranged parallel to the surface of the single-crystal Au(001) substrate, and, according to previous data,[29] they form a square cell.

**4.2. Preparation of Silver Nanoparticles.** The method of resistive UHV evaporation of a high-purity metal wire, wrapped around a previously thoroughly outgassed tungsten filament, was used to deposit silver onto the surface of the grown organic $CuPcF_4$ film, which was at room temperature. No further temperature treatment was applied to the sample.


https://dx.doi.org/10.1021/acsomega.0c00391
ACS Omega 2020, 5, 10441−10450

The metal deposition rate, measured using a quartz thickness gauge, was 1−2 Å/min.

The samples for TEM and HR-TEM investigations were prepared similarly to the methodology described in previous studies.[29,32] Cleaved NaCl single crystals were used as the substrate, and here, all of the parameters—temperature, rate of $CuPcF_4$ deposition, organic film thickness, rate of silver deposition, and nominal silver coverage—were the same as for the systems grown on the Au(001) surface. Then, to fix the resulting nanocomposite thin films ($Ag/CuPcF_4$), they were coated with an ultrathin layer of amorphous carbon, cut into square pieces with sides of about 3 mm, separated from NaCl by immersion in distilled water, and transferred to 250-mesh (250 lines/inch) copper grids for further electron microscopic studies.

**4.3. TEM Investigations.** To verify the presence of NPs in the organic film as well as to reveal their mean size and size distribution along with the shape and the crystalline structure, we used transmission electron microscopy by means of a JEM 100 CX operated at 100 keV as well as high-resolution transmission electron microscopy using a JEM 2100 operated at 200 keV.

**4.4. Photoemission and Absorption Soft X-ray Spectroscopy.** Electronic structures (CL, VB, and empty states) of nanocomposites were studied as a function of nominal silver deposition under UHV conditions using X-ray photoelectron spectroscopy and NEXAFS techniques at the RGBL beamline of BESSY II synchrotron radiation facility (Berlin, Germany). Partly, the CL measurements were performed at the I311 beamline of the MAX IV Laboratory (Lund, Sweden) as well as at the P04 beamline of PETRA III (DESY, Hamburg, Germany). The samples were studied in situ right after silver deposition on the $CuPcF_4$ film grown on the Au(001) crystal.

## AUTHOR INFORMATION


### Corresponding Author

**Victor Yu. Aristov** − *Deutsches Elektronen-Synchrotron DESY, 22607 Hamburg, Germany; Institute of Solid State Physics of Russian Academy of Sciences, 142432 Chernogolovka, Russia;* orcid.org/0000-0002-9596-9898; Email: victor.aristov@desy.de

### Authors

**Olga V. Molodtsova** − *Deutsches Elektronen-Synchrotron DESY, 22607 Hamburg, Germany; ITMO University, 197101 Saint Petersburg, Russia*

**Irina M. Aristova** − *Institute of Solid State Physics of Russian Academy of Sciences, 142432 Chernogolovka, Russia*

**Dmitrii V. Potorochin** − *Deutsches Elektronen-Synchrotron DESY, 22607 Hamburg, Germany; ITMO University, 197101 Saint Petersburg, Russia; Institut für Experimentelle Physik, D-09596 Freiberg, Germany; Europian XFELGmbH, D-22869 Schenefeld, Germany*

**Sergey V. Babenkov** − *Deutsches Elektronen-Synchrotron DESY, 22607 Hamburg, Germany; Institut für Physik, Johannes Gutenberg-Universität, D-55099 Mainz, Germany*

**Igor I. Khodos** − *Institute of Microelectronics Technology and High-Purity Materials of Russian Academy of Sciences, 142432 Chernogolovka, Russia*

**Serguei L. Molodtsov** − *ITMO University, 197101 Saint Petersburg, Russia; Institut für Experimentelle Physik, D-09596 Freiberg, Germany; Europian XFELGmbH, D-22869 Schenefeld, Germany*

**Anna A. Makarova** − *Institute of Chemistry and Biochemistry, Free University of Berlin, D-14195 Berlin, Germany*

**Dmitry A. Smirnov** − *Institut für Festkörper- und Materialphysik, Technische Universität Dresden, 01062 Dresden, Germany*

Complete contact information is available at: https://pubs.acs.org/10.1021/acsomega.0c00391


### Notes

The authors declare no competing financial interest.

## ACKNOWLEDGMENTS

This work was carried out within the state task of ISSP RAS and supported by the Russian Foundation for Basic Research (Grant No. 20-02-00489). We are grateful to all staff members of the following beamlines: RGBL at BESSY II (Berlin), P04 at PETRA III (Hamburg), and I311 at MAX IV Laboratory (Lund).

## REFERENCES


(1) Wang, Z. W.; Palmer, R. E. Chapter 6—Atomic-Scale Structure Analysis by Advanced Transmission Electron Microscopy. *Front. Nanosci.* **2015**, *9*, 127−154.

(2) Li, Z. Chapter 5—Scanning Transmission Electron Microscopy Studies of Mono- and Bimetallic Nanoclusters. *Front. Nanosci.* **2012**, *3*, 213−247.

(3) Wang, G. Nanotechnology: The New Features. 2018, arXiv:physics/1812.04939 v1 [cs.ET]. arXiv.org e-Print archive. https://arxiv.org/abs/1812.04939.

(4) Taylor, M. G.; Mpourmpakis, G. Thermodynamic stability of ligand-protected metal nanoclusters. *Nat. Commun.* **2017**, *8*, No. 15988.

(5) Poddubny, A.; Iorsh, I.; Belov, P.; Kivshar, Y. Hyperbolic metamaterials. *Nat. Photonics* **2013**, *7*, 948−957.

(6) Takayama, O.; Sukham, J.; Malureanu, R.; Lavrinenko, A. V.; Puentes, G. Photonic spin Hall effect in hyperbolic metamaterials at visible wavelengths. *Opt. Lett.* **2018**, *43*, 4602−4605.

(7) Yun, J. Ultrathin metal films for transparent electrodes of flexible optoelectronic devices. *Adv. Funct. Mater.* **2017**, *27*, No. 1606641.

(8) Lu, H.; Ren, X.; Ouyang, D.; Choy, W.C.H. Emerging novel metal electrodes for photovoltaic applications. *Small* **2018**, *14*, No. 1703140.

(9) Bi, Y.-G.; Feng, J.; Ji, J.-H.; Chen, Y.; Liu, Y.-S.; Li, Y.-F.; Liu, Y.-F.; Zhang, X.-L.; Sun, H.-B. Ultrathin and ultrasmooth Au films as transparent electrodes in ITO-free organic light-emitting devices. *Nanoscale* **2016**, *8*, 10010−10015.

(10) Malureanu, R.; Lavrinenko, A. Ultra-thin films for plasmonics: a technology overview. *Nanotechnol. Rev.* **2015**, *4*, 259−275.

(11) Yakubovsky, D. I.; Stebunov, Y. V.; Kirtaev, R. V.; Voronin, K. V.; Voronov, A. A.; Arsenin, A. V.; Volkov, V. S. Graphene-supported thin metal films for nanophotonics and optoelectronics. *Nanomaterials* **2018**, *8*, 1058.

(12) Jang, H.-S.; Seong, B.; Zang, X.; Lee, H.; Bae, J. W.; Cho, D.-H.; Kao, E.; Yang, C.; Kang, G.; Liu, Y.; Park, H. P.; Byun, D.; Lin, L. Ultrafast Growth of Large 2D Silver Nanosheets by Highly Ordered Biological Template at Air/Gel Interface. *Adv. Mater. Interfaces* **2018**, *5*, No. 1701491.

(13) Musick, K. M.; Rigosa, J.; Narasimhan, S.; Wurth, S.; Capogrosso, M.; Chew, D. J.; Fawcett, J. W.; Micera, S.; Lacour, S. P. Chronic multichannel neural recordings from soft regenerative microchannel electrodes during gait. *Sci. Rep.* **2015**, *5*, No. 14363.

(14) Yakubovsky, D. I.; Stebunov, Y. V.; Kirtaev, R. V.; Ermolaev, G. A.; Mironov, M. S.; Novikov, S. M.; Arsenin, A. V.; Volkov, V. S. Ultrathin and ultrasmooth gold films on monolayer MoS2. *Adv. Mater. Interfaces* **2019**, *6*, No. 1900196.

(15) Mir, S. H.; Nagahara, L. A.; Thundat, T.; Mokarian-Tabari, P.; Furukawa, H.; Khosla, A. Review: Organic-Inorganic Hybrid Functional Materials: An Integrated Platform for Applied Technologies. *J. Electrochem. Soc.* **2018**, *165*, B3137−B3156.
(16) Ma, L. P.; Liu, J.; Pyo, S.; Yang, Y. Organic bistable light-emitting devices. *Appl. Phys. Lett.* **2002**, *80*, 3018.
(17) Prime, D.; Paul, S.; Josephs-Franks, P. W. Gold nanoparticle charge trapping and relation to organic polymer memory devices. *Philos. Trans. R. Soc., A* **2009**, *367*, 4215−4225.
(18) Pan, F.; Gao, S.; Chen, C.; Song, C.; Zeng, F. Recent progress in resistive random access memories: Materials, switching mechanisms, and performance. *Mater. Sci. Eng., R* **2014**, *83*, 1−59.
(19) Bozano, L. D.; Kean, B. W.; Beinhoff, M.; Carter, K. R.; Rice, P. M.; Campbell Scott, J. Organic materials and thin-film structures for cross-point memory cells based on trapping in metallic nanoparticles. *Adv. Funct. Mater.* **2005**, *15*, 1933−1939.
(20) Yang, Y.; Ouyang, J.; Ma, L.; Tseng, R. J.-H.; Chu, C.-W. Electrical switching and bistability in organic/polymeric thin films and memory devices. *Adv. Funct. Mater.* **2006**, *16*, 1001−1014.
(21) Liu, Z.; Yasseri, A. A.; Lindsey, J. S.; Bocian, D. F. Molecular memories that survive silicon device processing and real-world operation. *Science* **2003**, *302*, 1543−1545.
(22) Scott, J. C. Is there an immortal memory? *Science* **2004**, *304*, 62−63.
(23) Ranganathan, K.; Wamwangi, D.; Coville, N. J. Plasmonic Ag nanoparticle interlayers for organic photovoltaic cells: An investigation of dielectric properties and light trapping. *Solar Energy* **2015**, *118*, 256−266.
(24) Jeong, S. H.; Choi, H.; Kim, J. Y.; Lee, T. W. Silver-Based Nanoparticles for Surface Plasmon Resonance in Organic Optoelectronics. *Part. Part. Syst. Charact.* **2015**, *32*, 164−175.
(25) Kuzumoto, Y.; Matsuyama, H.; Kitamura, M. Partially fluorinated copper phthalocyanine toward band engineering for high-efficiency organic photovoltaics. *Jpn. J. Appl. Phys.* **2014**, *53*, No. 01AB03.
(26) Klyamer, D. D.; Basova, T. V.; Krasnov, P. O.; Sukhikh, A. S. Effect of fluorosubstitution and central metals on the molecular structure and vibrational spectra of metal phthalocyanines. *J. Mol. Struct.* **2019**, *1189*, 73−80.
(27) Yoon, S. M.; Song, H. J.; Hwang, I.-C.; Kim, K. S.; Choi, H. C. Single crystal structure of copper hexadecafluorophthalocyanine (F16CuPc) ribbon. *Chem. Commun.* **2010**, *46*, 231−233.
(28) Kuzumoto, Y.; Matsuyama, H.; Kitamura, M. Structural and electrical properties of fluorinated copper phthalocyanine toward organic photovoltaics: Post-annealing effect under pressure. *Jpn. J. Appl. Phys.* **2014**, *53*, No. 04ER16.
(29) Babenkov, S. V.; Molodtsova, O. V.; Aristova, I. M.; Tchaplyguine, M.; Molodtsov, S. L.; Aristov, V. Yu. Hybrid organic-inorganic systems formed by self-assembled gold nanoparticles in $CuPcF_4$ molecular crystal. *Org. Electron.* **2016**, *32*, 228−236.
(30) Van Hove, M. V.; Koestner, R.; Stair, P.; Biberian, J.; Kesmodel, L.; Bartos, I.; Somorjai, G. The surface reconstructions of the (100) crystal faces of iridium, platinum and gold: I. experimental observations and possible structural models. *Surf. Sci.* **1981**, *103*, 189−217.
(31) Van Hove, M. V.; Koestner, R.; Stair, P.; Biberian, J.; Kesmodel, L.; Bartos, I.; Somorjai, G. The Surface Reconstructions of the (100) Crystal Faces of Iridium, Platinum and Gold: II. Structural Determination by {LEED} Intensity Analysis. *Surf. Sci.* **1981**, *103*, 218−238.
(32) Aristov, V. Y.; Molodtsova, O. V.; Laubschat, C.; Zhilin, V. M.; Aristova, I. M.; Kveder, V. V.; Knupfer, M. Properties of hybrid organic-inorganic systems: Au nanoparticles embedded into an organic CuPc matrix. *Appl. Phys. Lett.* **2010**, *97*, No. 113103.
(33) Shchukin, V. A.; Bimberg, D. Spontaneous ordering of nanostructures on crystal surfaces. *Rev. Mod. Phys.* **1999**, *71*, 1125−1171.
(34) Plyusnin, N. I. Formation of a Nanophase Wetting Layer and Metal Growth on a Semiconductor. *Tech. Phys. Lett.* **2018**, *44*, 980−983.
(35) Kukushkin, S. A.; Osipov, A. V.; Schmitt, F.; Hess, P. The nucleation of coherent semiconductor islands during the Stranski-Krastanov growth induced by elastic strains. *Semiconductors* **2002**, *36*, 1097−1105.
(36) Teys, S. A. Atomic Processes in the Formation of Strained Ge Layers on Si. In *Advances in Semiconductor Nanostructures: Growth, Characterization, Properties and Applications*; Latyshev, A. V.; Dvurechenskii, A. V.; Aseev, A. L., Eds.; Elsevier Inc., 2016.
(37) Park, K. T.; Miller, A.; Klier, K.; Opila, R. L.; Rowe, J. E. Heteroepitaxial copper phthalocyanine on Au(0 0 1) studied by high-resolution X-ray photoelectron spectroscopy. *Surf. Sci.* **2003**, *529*, L285−L292.
(38) Mazzone, A. M. Coalescence of metallic clusters: a study by molecular dynamics. *Philos. Mag. B* **2000**, *80*, 95−111.
(39) Lehtinen, K.E.J.; Zachariah, M. R. Effect of coalescence energy release on the temporal shape evolution of nanoparticles. *Phys. Rev. B* **2001**, *63*, No. 205402.
(40) Arcidiacono, S.; Bieri, N. R.; Poulikakos, D.; Grigoropoulos, C. P. On the coalescence of gold nanoparticles. *Int. J. Multiphase Flow* **2004**, *30*, 979−994.
(41) Molodtsova, O. V.; Aristova, I. M.; Babenkov, S. V.; Vilkov, O. V.; Aristov, V. Yu. Morphology and properties of a hybrid organic-inorganic system: Al nanoparticles embedded into CuPc thin film. *J. Appl. Phys.* **2014**, *115*, No. 164310.
(42) Lozzi, L.; Santucci, S. Au/CuPc interface: a valence band photoemission investigation. *J. Chem. Phys.* **2011**, *134*, No. 114709.
(43) Lozzi, L.; Santucci, S.; La Rosa, S. Au/CuPc interface: Photoemission investigation. *J. Vac. Sci. Technol., A* **2004**, *22*, 1477−1481.
(44) Aristov, V. Y.; Molodtsova, O. V.; Ossipyan, Yu. A.; Doyle, B. P.; Nannarone, S.; Knupfer, M. Ferromagnetic cobalt and iron top contacts on an organic semiconductor: Evidence for a reacted interface. *Org. Electron.* **2009**, *10*, 8−11.
(45) Peisert, H.; Knupfer, M.; Fink, J. Electronic structure of partially fluorinated copper phthalocyanine ($CuPCF_4$) and its interface to Au(100). *Surf. Sci.* **2002**, *515*, 491−498.
(46) Aristov, V. Y.; Molodtsova, O. V.; Maslyuk, V. V.; Vyalikh, D. V.; Zhilin, V. M.; Ossipyan, Y. A.; Bredow, T.; Mertig, I.; Knupfer, M. Electronic structure of the organic semiconductor copper phthalocyanine: experiment and theory. *J. Chem. Phys.* **2008**, *128*, No. 034703.
(47) Aristov, V. Y.; Bertolo, M.; Jacobi, K.; Maca, F.; Scheffler, M. Experimental and theoretical investigation of the electronic structure of silver deposited onto InSb(110) at 10 K. *Phys. Rev. B* **1993**, *48*, 5555−5566.


https://dx.doi.org/10.1021/acsomega.0c00391
*ACS Omega* 2020, 5, 10441−10450